Published in final edited form as:
Sci Signal. ; 5(250): ra81. doi:10.1126/scisignal.2003152.

Single Amino Acid Substitutions Confer the Antiviral Activity of the TRAF3 Adaptor Protein onto TRAF5

Peng Zhang[1], **Anna Reichardt**[2,*], **Huanhuan Liang**[1,*], **Roghiyh Aliyari**[2], **David Cheng**[2], **Yaya Wang**[2], **Feng Xu**[2], **Genhong Cheng**[2], and **Yingfang Liu**[1]

Genhong Cheng: gcheng@mednet.ucla.edu; Yingfang Liu: liuy@ibp.ac.cn

[1]State Key Laboratory of Biomacromolecules, CAS Key Laboratory of Infection and Immunity, Institute of Biophysics, Chinese Academy of Science, Beijing 100101, China

[2]Department of Microbiology, Immunology and Molecular Genetics, University of California, Los Angeles, CA 90095, USA

Abstract

The TRAF [tumor necrosis factor receptor–associated factor] family of cytoplasmic adaptor proteins link cell-surface receptors to intracellular signaling pathways that regulate innate and adaptive immune responses. In response to activation of RIG-I (retinoic acid–inducible gene I), a component of a pattern recognition receptor that detects viruses, TRAF3 binds to the adaptor protein Cardif [caspase activation and recruitment domain (CARD) adaptor–inducing interferon-b (IFN-b)], leading to induction of type I IFNs. We report the crystal structures of the TRAF domain of TRAF5 and that of TRAF3 bound to a peptide from the TRAF-interacting motif of Cardif. By comparing these structures, we identified two residues located near the Cardif binding pocket in TRAF3 (Tyr440 and Phe473) that potentially contributed to Cardif recognition. In vitro and cellular experiments showed that forms of TRAF5 with mutation of the corresponding residues to those of TRAF3 had TRAF3-like antiviral activity. Our results provide a structural basis for the critical role of TRAF3 in activating RIG-I–mediated IFN production.

Introduction

The tumor necrosis factor (TNF) receptor–associated factor (TRAF) family of adaptor proteins promotes the activation of several transcription factors to induce immune and inflammatory responses, including nuclear factor kB (NF-kB), activator protein-1 (AP-1), and interferon (IFN) regulatory factors 3 and 7 (IRF3/7), which are especially important for innate immune antiviral function (1, 2). Mammalian cells have six TRAF proteins, TRAF1 to TRAF6, all of which contain a conserved TRAF domain at the C terminus consisting of a

Correspondence to: Genhong Cheng, gcheng@mednet.ucla.edu; Yingfang Liu, liuy@ibp.ac.cn.

*These authors contributed equally to this work.

Author contributions: Constructs, protein expression and purification, and crystallization were performed by P.Z. Cell assays were performed by A.R., R.A., D.C., Y.W., and F.X. Data collection and structure determination were performed by H.L. Data analyses were performed by H.L., Y.L., and G.C. The manuscript was prepared by A.R. and H.L. and modified by Y.L. and G.C.

Competing interests: The authors declare that they have no competing interests.

Data and materials availability: The atomic coordinates have been deposited in the Protein Data Bank with the accession codes 4GHU and 4GJH.

coiled-coil domain followed by a TRAF-C domain; five (TRAF2 to TRAF6) also have an N-terminal RING domain and zinc finger motifs.

Despite high sequence homology, TRAF proteins associate with different ligands and carry out nonredundant functions (3). TRAF proteins are recruited directly or indirectly by various pattern recognition receptors, whereupon they recruit additional factors that activate the inhibitor of kB kinase (IKK) complex to trigger NF-kB activation (1). In addition, TRAF2, TRAF5, and TRAF6 can promote the activation of mitogen-activated protein kinase and c-Jun N-terminal kinase (2, 4), and TRAF3, TRAF5, and TRAF6 can mediate secretion of type I IFNs (5, 6). The molecular specificities that determine the individual TRAF protein functions, including the role of TRAF3 in stimulating IFN secretion, however, still remain incompletely defined.

On recognition of viral infection, TRAF3 is activated and primes the TRAF family member–associated NF-kB activator (TANK)–binding kinase 1 (TBK1) and IKKe complex to phosphorylate IRF3/7 (1, 7). Two major antiviral pathways activate TRAF3 (and type I IFN secretion): a Toll-like receptor (TLR)–dependent pathway and a TLR-independent pathway that are active in immune and nonimmune cells, respectively. In nonimmune cells, upon recognition of intracellular double-stranded RNA, cytoplasmic RNA helicases including retinoic acid–inducible gene I (RIG-I), helicard, and melanoma differentiation–associated protein 5 (MDA5) recruit the adaptor protein Cardif, which in turn recruits and activates TRAF3 (6, 8).

Cardif functions as a scaffolding protein, helping to coordinate the assembly of larger protein complexes that trigger downstream production of IFN and various other cytokines. The TRAF-interacting motif (TIM) of Cardif has been mapped to three regions, including the TRAF2 binding motif (T2BM) 143PVQDT147, TRAF6 binding motif 1 (T6BM1) 153PVENSE159, and TRAF6 binding motif 2 (T6BM2) 431PEENEY437 (9). Multiple TRAF-family proteins, including TRAF2, TRAF3, TRAF5, and TRAF6, have been identified as possible Cardif-binding partners and have been suggested to mediate IFN secretion downstream of Cardif. Previous studies from our group demonstrated direct interactions between the TRAF domain of TRAF3 and the T2BM of Cardif; subsequently, TRAF3 was also shown to interact with Cardif through the T6BM2 region (8, 10). In addition, TRAF6 is critical for IFN gene activation and has been suggested to be another regulator of IFN activation (5, 11, 12). However, we have shown that no other TRAF family-member TRAF domain, including TRAF5, can functionally replace the antiviral activity of TRAF3 (8). A hybrid form of TRAF5 containing the TRAF domain of TRAF3 gains antiviral activity, and conversely, substitution of the TRAF domain of TRAF5 into TRAF3 abrogates the antiviral function of TRAF3 (8). These data suggest that the functional specificity between TRAF3 and TRAF5 is determined by the TRAF domain.

Crystal structures of the TRAF domains of TRAF2, TRAF3, and TRAF6 in association with various TIMs have been determined, including crystal structures of the TRAF domain of TRAF3 bound to five ligands: CD40, lymphotoxin-b receptor (LTbR), B cell–activating factor receptor (BAFF-R), TANK, and latent membrane protein 1 (LMP1) (13–20). Within the common TRAF protein fold, TRAF domains form trimers with an aggregate structure

that is often compared to a mushroom. N-terminal coiled-coil motifs form the mushroom's "stalk"; high sequence conservation within these coiled-coil motifs allows TRAF proteins to form both homo and heterotrimers with other TRAFs. C-terminal TRAF-C domains form the mushroom's "cap" by folding into eight-stranded b-sandwiches that contain solvent-restricted binding crevices. These crevices serve as binding surfaces and measure about 15 Å∼ 19 Å∼ 22 Å, which can accommodate peptides about 20 amino acids long (21). Within this b-sandwich region, TRAF crystal structures have defined three structural "hotspots" shared within the TRAF family: a hydrophobic pocket, a set of serine fingers, and a grouping of polar residues (21). Subtle structural differences in this b-sandwich region and the hotspot residues account for the selective recruitment of various TRAF family members to binding partners. The TRAF domains of TRAF3 and TRAF5 show up to 65% sequence homology, and the hotspot residues are the same in these two proteins. However, the mechanisms and the specific amino acids responsible for the specificity of TRAF3 in the Cardif-mediated induction of IFN production remain to be elucidated.

Here, we report the crystal structures of the TRAF domain of TRAF5 and that of TRAF3 bound to a peptide from the TIM of Cardif. By comparing the structure of the TRAF3-Cardif complex to that of TRAF5, we found two residues in corresponding structural positions in TRAF3 and TRAF5 that differ and determine the binding abilities of TRAF3 and TRAF5 to Cardif. Mutations of these two residues in TRAF5 to the corresponding TRAF3 residues conferred TRAF3-like antiviral activity on the mutated TRAF5 proteins. Our results have determined a fundamental structure-based mechanism for the selectivity of TRAF3 in promoting the RIG-I–mediated IFN response.

Results

Configuration of the TRAF3-Cardif Complex

First, we sought to identify the TRAF binding site in Cardif that mediates direct interaction with the TRAF domain of TRAF3. We purified the TRAF domains of TRAF3 and TRAF5 as well as glutathione S-transferase (GST)–tagged peptides containing the TRAF binding sites of Cardif: residues 138 to 153 (138PSCPKPVQDTQPPESP153, which encompasses T2BM), residues 149 to 163 (149PPESPVENSEQALQT163, which encompasses T6BM1), and residues 425 to 441 (425SEPNHGPEENEYSSFRI441, which encompasses T6BM2). The GST-tagged Cardif peptides were bound to glutathione beads and incubated with the purified TRAF domains of TRAF3 and TRAF5. Only T2BM directly associated with the TRAF domain of TRAF3, and none of the three identified TRAF binding domains in Cardif directly associated with the TRAF domain of TRAF5 (fig. S1). Because T2BM contains a conserved PXQXT sequence, which has been speculated to be a TRAF3 binding motif, our result that T2BM was the relevant TRAF binding domain in Cardif was not surprising (1). Because Pro153 has been reported to be the first residue in T6BM1, we chose to use a slightly longer Cardif peptide (residues 138 to 158) that included the T2BM and T6BM1 motifs for further cocrystallization studies with TRAF3.

We purified the recombinant TRAF domain of TRAF3 (residues 376 to 565) and synthesized a peptide containing the TIM sequence of Cardif (residues 138 to 158) (8). Equimolar amounts of the TRAF3 and Cardif peptides were mixed and cocrystallized.

Crystals obtained were diffracted to 2.3 Å. The TRAF3-Cardif crystal adopted a P321 space group with one complex in an asymmetric unit; its structure was calculated by molecular replacement method, with the TRAF domain of TRAF3 as an initial searching model. Table 1 gives a summary of crystallographic data and refinement statistics. The Cardif peptide is observed in the Fo − Fc map: The Cardif peptide binds to TRAF3 at the edge of the b-sandwich crevice with a stoichiometry of 1:1 (Fig. 1A). After extensive refinement, 10 amino acids from Cardif including the sequence 138PSCPKPVQDT147 were unambiguously built for the backbone and side chains (Fig. 1B). Electron density plots for 148QPPE151 had poor resolution, suggesting that the C terminus of the Cardif peptide is flexible. The Gln148 of Cardif has alternative confirmations (fig. S2). However, from the structure, these different conformations of Gln148 do not substantially influence the binding of Cardif peptide with TRAF3. To identify the smallest peptide capable of binding TRAF3, we further truncated the Cardif peptide. Because pulldown assays indicated that the 13-residue peptide observed in the crystal structure (including residues 138 to 150) was sufficient for TRAF3 recruitment, we used this peptide for subsequent in vitro functional assays.

Previous reports have determined that the edge of the b-sandwich TRAF-C domain of TRAF3 is a key docking site for mediating ligand interactions in NF-kB pathways (21). Crystal structures of the TRAF domain of TRAF3 indicate that ligand peptides adopt one of two conformations within this crevice (21). The TIMs of CD40 and LTbR present with an imbedded “hairpin” configuration; in comparison, the TIMs of BAFF-R, TANK, and LMP1 present with a more open “boomerang” configuration. Our structure showed that similar to BAFF-R, TANK, and LMP1, the TIM of Cardif adopts an open conformation in the TRAF crevice of TRAF3 (Fig. 1C). Although it is not clear why the different ligands adopt different conformations, we suggest that TRAF3 uses the same crevice when binding to its ligand Cardif in the IFN pathway.

Interactions between the TRAF domain of TRAF3 and the TIM of Cardif

We structurally mapped the TRAF3-Cardif binding interface. The residues 143PVQDT147 in Cardif mediate the interaction with TRAF3; similar to the PXQXT peptides in CD40, TANK, and LMP1 (15, 16, 19), these five residues bind the conserved crevices of the b-sandwich region (Fig. 1, C and D). Our structure defined on a molecular level the specific interactions that these Cardif residues form with TRAF3's three hotspot clusters in the crevices. Phe474, Phe511, and Phe520 in TRAF3 form a hydrophobic pocket that binds Pro143 (in the sequence 143PVQDT147) in Cardif. The serine residues Ser517, Ser518, and Ser519 in TRAF3 determine a set of serine fingers that form a network of hydrogen bonds to Gln145 (in the sequence 143PVQDT147) in Cardif. Three additional TRAF3 residues—Arg456, Tyr458, and Asp462—define a hydrophilic region that generates multiple dipole-dipole interactions with Cardif. The guanidinium group of Arg456 and the hydroxyl group of Tyr458 hydrogen-bond to a carboxyl group on Asp146 in Cardif (in the sequence 143PVQDT147); the carboxyl group of Asp462 interacts with the amine and hydroxyl groups of Thr147 in Cardif (143PVQDT147). Our structure provides a means by which the point mutation T147I in Cardif disrupts its interaction with TRAF3: T147I in Cardif disrupts

a critical hydrogen bond that forms between Asp462 of TRAF3 and a carbonyl group of Thr147 in wild-type Cardif (8).

Our structure also located molecular interactions important for TRAF3-Cardif binding that involved the sequence 143PVQDT147 in Cardif but were independent of the conserved hotspot residues of TRAF3 (Fig. 1D). The carboxyl group of Gly532 in TRAF3 hydrogen-bonds to the amino group of Val144 in Cardif (in the sequence 143PVQDT147). Ser531 in TRAF3 provides an amino group that hydrogen-bonds to the carboxyl group of Val144 in Cardif (in the sequence 143PVQDT147). Ala530 in TRAF3 provides a carboxyl group that hydrogen-bonds to the amino group of Asp146 in Cardif (in the sequence 143PVQDT147). Unexpectedly, we observed a disulfide bond between Cys533 in TRAF3 and Cys160 in Cardif in our structure's electron density map (Fig. 1D). However, we believe that this covalent bond is an artifact that most likely formed as a result of oxidation that occurred during the crystallization process.

Structure of the TRAF domain of TRAF5

We determined the crystal structure of the TRAF domain of TRAF5 with a molecular replacement method, starting with the C-TRAF domain of TRAF3 as an initial model. To obtain a well-diffracted crystal, we truncated our TRAF5 construct at the N-TRAF domain, so that the construct covered residues 381 through the C-terminal end of TRAF5 (Fig. 2A). The crystal adopts a P212121 space group, with three molecules in one asymmetric subunit. Summaries of crystallographic data and refinement statistics are presented in Table 1. Our structure showed that TRAF5 forms a homotrimer with the typical mushroom-like structure that is characteristic of TRAF proteins. N-terminal coiled-coil motifs (TRAF5 residues 381 to 399) fold into the a helices that form the mushroom's stalk. The mushroom's cap is composed of an eight-stranded b-sandwich fold, consisting of residues 405 to 558. The two layers of an antiparallel b strand, b1 to b8, form a hydrophobic core.

The C-terminal 150 amino acids of TRAF3 and TRAF5 share 65% identity (Fig. 2B). When crystal structures of the C-terminal TRAF domains of TRAF3 (residues 416 to 567) and TRAF5 (residues 405 to 558) are superimposed, the main chain root mean square deviation (RMSD) between the TRAF domain of TRAF5 and that of TRAF3 is only 0.70 Å, suggesting that these two structures are very similar (Fig. 2C). One clear distinction between the two structures is the angle between the stalk and the cap of the mushroom (Fig. 2C). We suggest that this is caused by different degrees of flexibility in the hinge regions between the stalk and the cap (residues 400 to 404) of the two molecules.

Our structure confirmed previously predicted hotspot clusters in the TRAF domain of TRAF5, and showed that these hotspots form crevices for binding adaptor proteins. Phe463, Phe500, and Phe509 form a hydrophobic pocket; Arg445, Tyr447, and Asp451 make up a polar pocket; and three sequential serine residues, Ser506, Ser507, and Ser508, form a set of hydrophilic “serine fingers” (Fig. 2, B and C). When we compared the crevice residues between the TRAF domain of TRAF3 and the TRAF domain of TRAF5, we found that the hotspot residues from TRAF3 and TRAF5 can be superimposed very well (Fig. 2C). Because TRAF5 cannot replace TRAF3 in the RIG-I–mediated type I IFN pathway (8), we

suggest that other critical residues located outside this well-characterized binding crevice are involved in mediating the specific binding of TRAF3 to Cardif.

Structural comparison of the TRAF domains of TRAF3 and TRAF5

To determine on a molecular level why the TIM of Cardif binds the TRAF domain of TRAF3 but not that of TRAF5, we analyzed the residues in TRAF3 and TRAF5 located near the Cardif binding crevice using sequence and structural alignment. Two residues drew our attention. The corresponding residues in TRAF3 are Phe473 and Tyr440 and in TRAF5 are Tyr462 and Phe429 (Fig. 2, B and C). Although both residues are aromatic amino acids and are located on the surface of the b-sandwich domain and not within the crevice, we predicted that these two nonconserved residue positions contributed to the different binding abilities of TRAF3 and TRAF5 for Cardif.

To determine whether Phe473 and Tyr440 in TRAF3 were necessary for the binding of TRAF3 to Cardif, we generated a panel of purified TRAF domain oligopeptides, which included wild-type TRAF3 and TRAF5, TRAF3 F473Y, TRAF3 Y440F, and TRAF3 F473Y/Y440F, and examined the interactions of these peptides with the GST-Cardif TIM fusion proteins. As expected, the Cardif TIM associated with a peptide corresponding to the TRAF domain of wild-type TRAF3 but not wild-type TRAF5 (Fig. 3A). In agreement with our structure-based prediction that Phe473 and Tyr440 in TRAF3 enable TRAF3 to bind Cardif, none of the TRAF3 mutant peptides (F473Y, Y440F, or F473Y/Y440F) associated with the TIM of Cardif (Fig. 3A).

We reasoned that if sequence differences between these two corresponding residue positions were indeed responsible for the dissimilar Cardif binding abilities of TRAF3 and TRAF5, then mutation of these residues in TRAF5 to the corresponding TRAF3 residues should confer TRAF3-like binding ability for Cardif on TRAF5. To test this hypothesis, we performed the GST-Cardif TIM pulldown assay with the TRAF5 Y462F, F429Y, and F429Y/Y462F TRAF domain peptides, as well as the wild-type TRAF3 and TRAF5 peptides. All three TRAF5 TRAF domain mutants, but not wild-type TRAF5, associated with the TIM of Cardif (Fig. 3A).

We also wanted to confirm that the full-length point-mutant TRAF5 proteins interacted with Cardif. We performed GST pulldowns using a GST-Cardif TIM incubated with lysates from 293T cells expressing wild-type TRAF3 or TRAF5 or full-length TRAF5 Y462F or TRAF5 F429Y. As expected, wild-type TRAF3, but not wild-type TRAF5, associated with the TIM of Cardif. In confirmation of our hypothesis that we could switch TRAF5 toward a more TRAF3-like Cardif-binding phenotype, both TRAF5 Y462F and TRAF5 F429Y interacted with the TIM of Cardif (Fig. 3B).

We were surprised that the two residue positions, Phe473 and Tyr440 in TRAF3 and Tyr462 and Phe429 in TRAF5, played such a central role in mediating interactions with Cardif. The TRAF3 mutant Y440Awas previously reported to have reduced ability to bind to Cardif (8). Unfortunately, our electron density map was unclear for the C-terminal region of the Cardif TIM motif, which is spatially situated to form potential interactions with the TRAF3 residue Tyr440 (fig. S2). In lieu of further structural evidence, we hypothesized that the phenol

moiety of Tyr440 forms a hydrogen bond with a carbonyl group on the main chain of Cardif, and that this interaction is destroyed upon replacement of Tyr440 with either a phenylalanine, as in TRAF5, or an alanine, as in the TRAFA3 Y440A mutant (Fig. 3C). Our in vitro pulldown experimental results confirmed this hypothesis. Cardif peptides with mutations in the C-terminal region, such as P149A, P149S, and P150A, showed reduced binding to TRAF3. Other mutants, such as Cardif 138–148 and P150S, did not bind to TRAF3 (fig. S3). These results show that the TRAF3 binding site in Cardif covers amino acid residues beyond just the minimum 143PVQDT147 motif.

Our TRAF3-Cardif structure indicated that there should be sufficient space around Phe473 in TRAF3 to accommodate substitution of a tyrosine residue, as in either TRAF3 F473Y or the corresponding residue in TRAF5, Tyr462. Although the structure did not show direct interactions between Phe473 in TRAF3 and the Cardif peptide, we wondered whether the phenol moiety of Phe462 played a role in disrupting interactions with Cardif. Our structure showed that in TRAF5, Phe462 lies adjacent to Asp451 (which corresponds to Asp462 in TRAF3). The carboxyl group of Asp462 in TRAF3 interacts with the amino group of Thr147 in Cardif, and disruption of this interaction is sufficient to ablate the formation of the TRAF3-Cardif complex (Fig. 3C). Therefore, we hypothesize that Tyr462 in TRAF5 interacts with Asp451, thereby blocking the formation of the TRAF5-Cardif complex by preventing the establishment of hydrogen bonds between Asp451 in TRAF5 and Thr147 in Cardif.

Abolished antiviral function of TRAF3 F473Y and Y440F mutants

Next, we tested whether variants of TRAF3 in which these two residues were mutated to the corresponding TRAF5 residues (TRAF3 F473Yand Y440F) retained antiviral function. Because Cardif is required to recruit TRAF3 upon viral RNA recognition in the TLR-independent IFN secretion pathway, we reasoned that the decreased binding abilities of the TRAF3 F473Y and Y440F mutants for Cardif would attenuate TRAF3-Cardif–dependent antiviral responses.

We reconstituted TRAF3−/− mouse embryo fibroblasts (MEFs) with wild-type TRAF3, wild-type TRAF5, TRAF3 F473Y, TRAF3 Y440F, or TRAF3 F473Y/Y440F (Fig. 4A). We assessed the production of type I IFNs by the reconstituted MEFs in response to infection with a form of vesicular stomatitis virus (VSV) that coexpresses green fluorescent protein (GFP) (Fig. 4B). Compared to cells reconstituted with wild-type TRAF3, those reconstituted with TRAF3 F473Y, Y440F, or F473Y/Y440F mutants showed reduced secretion of IFN-b after infection with VSV-GFP. Our results suggest that the TRAF3 F473Y and Y440F mutants abrogate type I IFN production on viral infection.

We next assessed the antiviral state of the reconstituted MEF cell lines after infection with VSV-GFP. We used GFP fluorescence as an indirect measure of viral replication and quantified it as the percentage of VSVGFP– positive cells (reflecting infection across a cell population) multiplied by the geometric mean of the fluorescence intensity (which accounts for the degree of infection within individual cells). As an additional validation, we used viral plaque assay to measure live, infectious virions as a direct measure of viral replication. As expected, cells reconstituted with wild-type TRAF3 were resistant to infection, evidenced by

both their low amounts of GFP fluorescence and low viral titers, whereas cells reconstituted with wild-type TRAF5 or vector were more susceptible to infection, as evidenced by both high amounts of GFP fluorescence and high viral titers (Fig. 4, C and D). Cells reconstituted with TRAF3 F473Y, Y440F, or F473Y/Y440F had an intermediate phenotype. They showed increased GFP fluorescence compared to wild-type TRAF3-reconstituted cells but less GFP fluorescence compared to cells reconstituted with wild-type TRAF5; similarly, their viral titers were about fivefold higher than those of cells reconstituted with wild-type TRAF3 but were twofold less than those of cells reconstituted with wild-type TRAF5 (Fig. 4, C and D).

Acquired antiviral function of TRAF5 F429Y and Y462F

Next, we tested whether mutation of these two TRAF5 residues to the corresponding TRAF3 residue (TRAF5 Y462F and F429Y) endowed TRAF5 with TRAF3-like antiviral function. Because Cardif is required for TRAF3 recruitment upon viral RNA recognition in the TLR-independent IFN secretion pathway, we theorized that the increased binding of the TRAF5 Y462F and F429Y mutants to Cardif could allow them to partially rescue TRAF3-dependent antiviral responses in TRAF3-deficient cells. We reconstituted TRAF3−/− MEFs with wild-type TRAF3, wildtype TRAF5, TRAF5 Y462F, and TRAF5 F429Y (Fig. 5A).

We assessed the production of type I IFNs by the reconstituted MEFs in response to infection with both Sendai virus and VSV-GFP (Fig. 5, B and C). Compared to cells reconstituted with wild-type TRAF3 and TRAF5, secretion of IFN-a and IFN-b after infection with Sendai virus and VSVGFP, respectively, was significantly increased in cells reconstituted with the TRAF5 Y462F or F429Y mutants as compared to cells reconstituted with wild-type TRAF5. Similarly, as compared to reconstitution with wildtype TRAF5, cells reconstituted with the TRAF5 Y462F or F429Y mutants showed increased expression of IFN-b mRNA and of IP10 and MX1 mRNAs (both of which are IFN-stimulated genes) at 8 and 12 hours after infection with VSV-GFP. Our results suggested that the TRAF5 Y462F and F429Y mutants restored type I IFN production on viral infection.

We also assessed the antiviral responses of the reconstituted MEFs by quantification of GFP fluorescence and viral titers after infection with VSV-GFP. As expected, cells reconstituted with wild-type TRAF3 were resistant to infection, evidenced by both their low GFP fluorescence and low viral titers, whereas cells reconstituted with wild-type TRAF5 or vector were more susceptible to infection, as evidenced by both high GFP fluorescence and high viral titers. TRAF5 Y462F– or TRAF5 F429Y–reconstituted cells had an intermediate phenotype: They showed increased GFP fluorescence compared to TRAF3-reconstituted cells but much less GFP fluorescence compared to cells reconstituted with wildtype TRAF5, and their viral titers were about 10-fold lower than those of cells reconstituted with wild-type TRAF5 (Fig. 5, D and E).

We also generated single-cell clones for each mutant and wild-type TRAF5 construct. Although cells in a polyclonal population express different amounts of reconstituted protein, individual cells within a clonal cell line will express the same amount of reconstituted protein. Polyclonal populations therefore examine an average phenotype (cells with uneven expression of TRAF3 or TRAF5 can exhibit a corresponding spectrum of phenotype), but

our experiments with the clonal cell lines allowed us to examine the effects of TRAF3 and TRAF5 at a given, uniform amount of expression. In agreement with our results using the polyclonal reconstituted cell lines, we found that clonal reconstitution with the TRAF5 Y462F or F429Y mutants, but not wild-type TRAF5, rescued resistance to VSV-GFP infection (Fig. 5F). Our findings suggest that, in agreement with our structure-based predictions, the TRAF5 Y462F or F429Y mutants can at least partially rescue resistance to VSV-GFP infection in TRAF3−/− MEFs.

Discussion

TRAF3 plays an important role in activating type I IFN secretion through both TLR-dependent and TLR-independent pathways (6). In the TLR independent pathway, cytoplasmic RNA sensors recruit the adaptor Cardif, which in turn associates with and activates TRAF3. The structural basis for the TRAF3-Cardif interaction is still not clear, although three potential TRAF binding sites in Cardif have been reported (9, 10). The recruitment of TRAF3 to Cardif is determined through its TRAF domain, and hybrid TRAF5 proteins containing the TRAF domain of TRAF3 gain the ability to bind to Cardif (8). Here, we present crystal structures of TRAF5 and the TRAF3-Cardif complex. Analysis of these structures has allowed us to dissect on the molecular level a structural basis for the interaction of TRAF3 with Cardif and its critical role in RIG-I–mediated type I IFN activation. Here, on the basis of crystal structure analysis and coprecipitation experiments, we suggest that TRAF3 can directly associate only with residues 138 to 153 of Cardif (138PSCPKPVQDTQPPESP153, which encompasses T2BM), and not with residues 151 to 165 or 425 to 439 of Cardif (which encompass T6BM1 and T6BM2, respectively).

Superposition of the TRAF3-Cardif and TRAF5 crystal structures allowed us to compare corresponding crevice residues between the TRAF domains of TRAF3 and TRAF5. We identified two residues that are not conserved between TRAF3 and TRAF5: The corresponding residues in TRAF3 are Phe473 and Tyr440 and in TRAF5 are Tyr462 and Phe429. The TRAF3 mutant Y440A was previously reported to have reduced Cardif binding (8). We reasoned that if sequence differences between these two corresponding residue positions were indeed responsible for the dissimilar abilities to bind to Cardif and the RIG-I–mediated antiviral activity of TRAF3 and TRAF5, then point mutations of these residues in TRAF5 to the corresponding TRAF3 residue should switch TRAF5 toward a TRAF3-like function. We showed that two point mutations in the TRAF domain of TRAF5, Y462F and F429Y, give TRAF5 a TRAF3-like function in Cardif binding and in regulating TLR-independent IFN secretion. Considering the different physiological roles of TRAF3 and TRAF5, it is interesting that a single amino acid substitution can switch TRAF5 toward a TRAF3-like specificity.

It will be interesting to investigate how and if these same sites in the TRAF domain of TRAF3 determine binding specificity to other TRAF3 binding partners. Ely et al. have reported that TRAF domain binding crevices undergo subtle structural adjustments when bound to different proteins (22). When human TRAF3 is recruited by TANK, they suggested that the phenyl ring of Tyr377 (corresponding to mouse residue Tyr440) rotates away from an adjacent b strand, thereby disrupting a salt bridge with Arg393 to form a new

hydrophobic interaction with Leu193. Given the role of TRAF3 in both TLR-dependent and TLR-independent type I IFN pathways, it will be interesting to determine the interactions between TRAF3 and its adaptors in the TLR-dependent pathway. Ligation of TLRs causes the recruitment of Toll/interleukin-1 receptor (TIR) domain–containing adaptor proteins, including myeloid differentiation primary response gene 88 (MyD88) and TIR domain–containing adaptor–inducing IFN-b (TRIF), to the signaling complex and triggers activation of downstream transcription factors. Whereas TLR3/4 (TLR3 and TLR4) and TLR7/8/9 trigger IFN secretion through a TRAF3-dependent process, TLR3/4 recruit TRAF3 through TRIF, and TLR7/8/9 recruit TRAF3 through the adaptor protein MyD88 (6, 23). It will be interesting to determine the residues in TRAF3 that mediate interactions between TRAF3 and MyD88 or TRIF, and to further characterize the possible dynamic structural adaptation these residues undergo to accommodate interactions with the diverse binding partners of TRAF3. It will also be interesting to learn whether the TRAF5 Y462F and F439Y mutants gain function in TLR-dependent IFN secretion, as well as other TRAF3-regulated signaling pathways including BAFF-R and alternative NF-kB activation.

Our results elucidate a structural basis for the selective role of TRAF3 within the TRAF family in promoting RIG-I–mediated type I IFN secretion. Because type I IFN has a pathogenic role for certain autoimmune disorders including systemic lupus erythematosus, a TRAF3 signaling blockade mediated through the TRIF and MyD88 adaptors could conceivably be a therapeutic target. However, because TRAF3 regulates so many signaling cascades, a complete blockade of TRAF3 signaling would have distinctly decreased utility. Further understanding of the structural specificities of TRAF3 for its various ligands, including Cardif, could allow the development of small-molecule therapeutics that are targeted to the ligand-binding pockets of TRAF3 and designed specifically to inhibit the interaction of TRAF3 with only a subset of ligands. Our results illustrate that by affecting interactions with signaling adaptors, even seemingly minor structural differences between TRAF family members can alter their function. Further analysis of how structural differences in TRAF proteins determine their specific functions will improve efforts to intelligently guide immunological responses to pathogens and autoimmune stimuli.

Materials and Methods

Constructs and protein expression and purification

The TRAF domain of mouse TRAF3 (residues 376 through the C terminus) was cloned into a pET21b vector (Invitrogen). The plasmid was transformed into Escherichia coli strain BL21(DE3) cells. Bacteria were cultured in LB medium at 310 K with ampicillin (100 mg/liter). When the absorbance at 600 nm (A600) reached 0.6 to 0.8, the culture was induced with 0.5 mM isopropyl-b-D-thiogalactopyranoside (IPTG); bacteria were harvested 4 hours after induction by centrifugation at 5000 rpm for 10 min. The pellet was resuspended with denaturing lysis buffer [6 M urea, 25 mM tris (pH 7.5), 5 mM imidazole, 5 mM b-mercaptoethanol] and lysed by sonication. The lysate was separated by centrifugation at 30,700g for 30 min. The supernatant was bound to Ni-NTA (nickel–nitrilotriacetic acid) beads (Qiagen Inc.) and washed several times with denaturing lysis buffer. TRAF3 was refolded in urea gradient buffer (4 to 0 M) with 25 mM tris at pH 7.5 and 5 mMb-

mercaptoethanol. To produce a shortened TRAF3 for crystallization, TRAF3 was digested by trypsin (1:1000 molecular ratio) for 4 hours at 277 K. The reaction was terminated by the addition of 1 mM phenylmethylsulfonyl fluoride (final concentration). The shortened TRAF3 was further purified by gel filtration with a Superdex 75 column (GE Healthcare Inc.) on fast-flow protein purification system.

The TRAF domain of TRAF5 (residues 365 through C terminus) was cloned into pGEX-6p-1. The plasmids were transformed to BL21(DE3) cells grown in LB-ampicillin medium at 37°C. When culture density reached 1.5 (A600), the bacteria were induced with 0.1 mM IPTG at 16°C for 24 hours. The bacteria were harvested by centrifugation at 7000g for 10 min and lysed under 15,000 psi in 20 mM tris (pH 7.5), 150 mM NaCl, 5 mM EDTA, 1 mM dithiothreitol (DTT). GST tags were cleaved by PreScission Protease at 4°C for 16 hours. The TRAF domain of TRAF5 was separated by gel filtration with Superdex 200 (GE Healthcare Inc.).

The Cardif peptide (138PSCPKPVQDTQPPESPVENSE158) used for cocrystallization with TRAF3 was purchased from GL Biochem Ltd. and was 99% pure.

Crystallization

For cocrystallization of Cardif with TRAF3, the Cardif peptide was dissolved in filtered water at 10 mg/ml and added to purified TRAF3. The ratio of Cardif peptides to TRAF3 was 1:1, and the final concentration was 3 to 4 mg/ml as confirmed by Coomassie blue staining of SDS–polyacrylamide gel electrophoresis (SDS-PAGE). Crystals were observed in multiple conditions as screened with the Crystal Screen and Index reservoir solutions (Hampton Research Inc.) with hanging drops at 289 K. The crystals grew to a hexagonal shape with usable size in the conditions of 0.1 M Hepes (pH 7.5), 10% polyethylene glycol 6000 (PEG6000), and 5% (v/v) 2-methyl-2,4-pentanediol.

The TRAF5 TRAF domain [crystallization buffer: 20 mM tris (pH 7.5), 150 mM NaCl, 5 mM EDTA, 1 mM DTT] was crystallized with 0.1 M ammonium acetate, 0.1 M bis-tris (pH 6.5), 15% (w/v) PEG10000 in a hanging-drop diffusion system at 16°C.

Crystallographic analysis

Diffraction data were collected at the Photon Factory, KEK (Japan) and Shanghai Synchrotron Radiation Facilities (SSRF, China). Crystals were flash-frozen before data collection with 10% glycerol. Data were processed by HKL2000 (24). The structure of TRAF5 was solved by Phaser (25) with a molecular replacement method. The native truncated TRAF3 atomic coordinates 2GKW were used as an initial model. The TRAF3/Cardif complex was refined with the native TRAF3 atomic coordinates. An Fo −Fc difference map was used to build the Cardif peptide. Structure refinement and model rebuilding were done iteratively with Phenix (26) and Coot (27). The Ramachandran plots were generated with Procheck (28); 97.44 and 2.56% of the amino acids in TRAF3/Cardif and 95.98 and 4.02% of the amino acids in TRAF5 were in the most favorable and additional allowed regions, respectively. No amino acids were in the disallowed region. The atomic coordinates and diffraction data have been deposited in the Protein Data Bank (4GHU for TRAF3/Cardif and 4GJH for TRAF5). All figures were prepared by Coot and

Pymol (http://www.pymol.org/). The angle between the N-terminal a helices in TRAF3 and TRAF5 in Fig. 2C was calculated with Pymol. The superposition is performed with Coot with the C-TRAF domains (TRAF3 416–559 and TRAF5 353–498).

Reagents

Anti-FLAG (M2) antibodies were obtained from Sigma. Anti-Hsp90a/b (H-114) antibodies were obtained from Santa Cruz Biotechnology. FuGENE 6 reagent was purchased from Roche. VSVs expressing GFP were gifts from G. Barber.

Constructs

GST-Cardif (TIM) was constructed as previously described (29). Murine TRAF3, TRAF5, and mutant constructs were generated as previously described in either pBABE-puromycin or pBABE-puro-TAP retroviral vectors with N-terminal FLAG tags (8). Single point mutants of TRAF3 and TRAF5 were constructed with a QuikChange kit (Stratagene) and the pBABE-puro-TAP-TRAF3 vector as template.

Cell culture and reconstitution

Human embryonic kidney (HEK) 293T cells were maintained in Dulbecco's modified Eagle's medium (Gibco) supplemented with 10% fetal bovine serum, penicillin (100 U/ml), and streptomycin (0.1 mg/ml). We performed transient transfection of HEK 293T cells using standard calcium phosphate methods. To reconstitute TRAF3−/− cells, we transfected HEK 293T cells with aMoloney murine leukemia virus-yA helper construct plus either pBABE-puro alone or the indicated pBABE-puro construct using FuGENE 6. TRAF3−/− cells were then infected with the filtered 293T cell supernatants and then selected with puromycin (5.0 mg/ml).

Immunoblotting

Cells were lysed in modified radioimmunoprecipitation assay buffer containing 0.5% (v/v) NP40 and 0.1% (w/v) sodium deoxycholate supplemented with protease inhibitor tablets (Roche). Equal amounts of whole-cell lysates were resolved by 8% SDS-PAGE and analyzed by Western blotting with the indicated antibodies.

GST pulldown assays

GST pulldown assays were performed as previously described (8). Glutathione beads (Sigma-Aldrich) were incubated with E. coli–expressed GST alone or GST-TIM for 12 hours. Glutathione beads were then washed and incubated for 12 hours with lysates of 293T cells expressing the indicated TRAF3 or TRAF5 constructs. For Fig. 3A and figs. S1 and S3, the TRAF3 or TRAF5 proteins were purified as described above. After being washed, proteins were eluted from the beads, resolved by 8% SDS-PAGE, and analyzed by Western blotting with the indicated antibodies, as described previously (8). All these results were confirmed by three independent experiments.

Viral inhibition assays

Viral inhibition experiments were performed as described previously (6). Reconstituted TRAF3−/− MEFs were infected with either VSV-GFP or Sendai virus; cell supernatants were collected 12 hours after infection for analysis by enzyme-linked immunosorbent assay, plaque assay, and measurement of GFP fluorescence.

Supplementary Material

Refer to Web version on PubMed Central for supplementary material.

Acknowledgments

We thank our colleague H. Wang for crystal data collection of TRAF5. We thank the staff at Photon Factory, KEK (Japan) and SSRF (China) for assistance in the use of the synchrotron resource.

Funding: This work was supported by grants to Y.L. from the Ministry of Science and Technology (2009CB522505, 2011CB910304, and 2012CB910204) and the National Science Foundation of China (30925011, 31030024, and 31021062), grants to G.C. from the NIH (R01GM078607 and R01AI069120), and an NSFC-NIH grant to Y.L. and G.C. (81261120407).

References and Notes

1. Wang Y, Zhang P, Liu Y, Cheng G. TRAF-mediated regulation of immune and inflammatory responses. Sci China Life Sci. 2010; 53:159–168. [PubMed: 20596822]
2. Häcker H, Tseng PH, Karin M. Expanding TRAF function: TRAF3 as a tri-faced immune regulator. Nat Rev Immunol. 2011; 11:457–468. [PubMed: 21660053]
3. Chung JY, Park YC, Ye H, Wu H. All TRAFs are not created equal: Common and distinct molecular mechanisms of TRAF-mediated signal transduction. J Cell Sci. 2002; 115:679–688. [PubMed: 11865024]
4. Bradley JR, Pober JS. Tumor necrosis factor receptor-associated factors (TRAFs). Oncogene. 2001; 20:6482–6491. [PubMed: 11607847]
5. Tang ED, Wang CY. TRAF5 is a downstream target of MAVS in antiviral innate immune signaling. PLoS One. 2010; 5:e9172. [PubMed: 20161788]
6. Oganesyan G, Saha SK, Guo B, He JQ, Shahangian A, Zarnegar B, Perry A, Cheng G. Critical role of TRAF3 in the Toll-like receptor-dependent and –independent antiviral response. Nature. 2006; 439:208–211. [PubMed: 16306936]
7. He JQ, Oganesyan G, Saha SK, Zarnegar B, Cheng G. TRAF3 and its biological function. Adv Exp Med Biol. 2007; 597:48–59. [PubMed: 17633016]
8. Saha SK, Pietras EM, He JQ, Kang JR, Liu SY, Oganesyan G, Shahangian A, Zarnegar B, Shiba TL, Wang Y, Cheng G. Regulation of antiviral responses by a direct and specific interaction between TRAF3 and Cardif. EMBO J. 2006; 25:3257–3263. [PubMed: 16858409]
9. Xu LG, Wang YY, Han KJ, Li LY, Zhai Z, Shu HB. VISA is an adapter protein required for virus-triggered IFN-b signaling. Mol Cell. 2005; 19:727–740. [PubMed: 16153868]
10. Paz S, Vilasco M, Werden SJ, Arguello M, Joseph-Pillai D, Zhao T, Nguyen TL, Sun Q, Meurs EF, Lin R, Hiscott J. A functional C-terminal TRAF3-binding site in MAVS participates in positive and negative regulation of the IFN antiviral response. Cell Res. 2011; 21:895–910. [PubMed: 21200404]
11. Yoshida R, Takaesu G, Yoshida H, Okamoto F, Yoshioka T, Choi Y, Akira S, Kawai T, Yoshimura A, Kobayashi T. TRAF6 and MEKK1 play a pivotal role in the RIG-I-like helicase antiviral pathway. J Biol Chem. 2008; 283:36211–36220. [PubMed: 18984593]
12. Konno H, Yamamoto T, Yamazaki K, Gohda J, Akiyama T, Semba K, Goto H, Kato A, Yujiri T, Imai T, Kawaguchi Y, Su B, Takeuchi O, Akira S, Tsunetsugu-Yokota Y, Inoue J. TRAF6

establishes innate immune responses by activating NF-kB and IRF7 upon sensing cytosolic viral RNA and DNA. PLoS One. 2009; 4:e5674. [PubMed: 19479062]

13. Park YC, Burkitt V, Villa AR, Tong L, Wu H. Structural basis for self-association and receptor recognition of human TRAF2. Nature. 1999; 398:533–538. [PubMed: 10206649]
14. Ye H, Park YC, Kreishman M, Kieff E, Wu H. The structural basis for the recognition of diverse receptor sequences by TRAF2. Mol Cell. 1999; 4:321–330. [PubMed: 10518213]
15. Ni CZ, Welsh K, Leo E, Chiou CK, Wu H, Reed JC, Ely KR. Molecular basis for CD40 signaling mediated by TRAF3. Proc Natl Acad Sci USA. 2000; 97:10395–10399. [PubMed: 10984535]
16. Li C, Ni CZ, Havert ML, Cabezas E, He J, Kaiser D, Reed JC, Satterthwait AC, Cheng G, Ely KR. Downstream regulator TANK binds to the CD40 recognition site on TRAF3. Structure. 2002; 10:403–411. [PubMed: 12005438]
17. Li C, Norris PS, Ni CZ, Havert ML, Chiong EM, Tran BR, Cabezas E, Reed JC, Satterthwait AC, Ware CF, Ely KR. Structurally distinct recognition motifs in lymphotoxin-b receptor and CD40 for tumor necrosis factor receptor associated factor (TRAF)-mediated signaling. J Biol Chem. 2003; 278:50523–50529. [PubMed: 14517219]
18. Ni CZ, Oganesyan G, Welsh K, Zhu X, Reed JC, Satterthwait AC, Cheng G, Ely KR. Key molecular contacts promote recognition of the BAFF receptor by TNF receptor-associated factor 3: Implications for intracellular signaling regulation. J Immunol. 2004; 173:7394–7400. [PubMed: 15585864]
19. Wu S, Xie P, Welsh K, Li C, Ni CZ, Zhu X, Reed JC, Satterthwait AC, Bishop GA, Ely KR. LMP1 protein from the Epstein-Barr virus is a structural CD40 decoy in B lymphocytes for binding to TRAF3. J Biol Chem. 2005; 280:33620–33626. [PubMed: 16009714]
20. Ye H, Arron JR, Lamothe B, Cirilli M, Kobayashi T, Shevde NK, Segal D, Dzivenu OK, Vologodskaia M, Yim M, Du K, Singh S, Pike JW, Darnay BG, Choi Y, Wu H. Distinct molecular mechanism for initiating TRAF6 signalling. Nature. 2002; 418:443–447. [PubMed: 12140561]
21. Ely KR, Li C. Structurally adaptive hot spots at a protein interaction interface on TRAF3. J Mol Recognit. 2002; 15:286–290. [PubMed: 12447905]
22. Ely KR, Kodandapani R, Wu S. Protein-protein interactions in TRAF3. Adv Exp Med Biol. 2007; 597:114–121. [PubMed: 17633021]
23. Häcker H, Redecke V, Blagoev B, Kratchmarova I, Hsu LC, Wang GG, Kamps MP, Raz E, Wagner H, Häcker G, Mann M, Karin M. Specificity in Toll-like receptor signalling through distinct effector functions of TRAF3 and TRAF6. Nature. 2006; 439:204–207. [PubMed: 16306937]
24. Otwinowski Z, Minor W. Processing of X-ray diffraction data collected in oscillation mode. Methods Enzymol. 1997; 276:307–326.
25. McCoy AJ, Grosse-Kunstleve RW, Adams PD, Winn MD, Storoni LC, Read RJ. Phaser crystallographic software. J Appl Crystallogr. 2007; 40:658–674. [PubMed: 19461840]
26. Adams PD, Afonine PV, Bunkóczi G, Chen VB, Davis IW, Echols N, Headd JJ, Hung LW, Kapral GJ, Grosse-Kunstleve RW, McCoy AJ, Moriarty NW, Oeffner R, Read RJ, Richardson DC, Richardson JS, Terwilliger TC, Zwart PH. PHENIX: A comprehensive Python-based system for macromolecular structure solution. Acta Crystallogr D Biol Crystallogr. 2010; 66:213–221. [PubMed: 20124702]
27. Emsley P, Lohkamp B, Scott WG, Cowtan K. Features and development of Coot. Acta Crystallogr D Biol Crystallogr. 2010; 66:486–501. [PubMed: 20383002]
28. Laskowski RA, MacArthur MW, Moss DS, Thornton JM. PROCHECK: A program to check the stereochemical quality of protein structures. J Appl Cryst. 1993; 26:283–291.
29. Saha SK, Cheng G. TRAF3: A new regulator of type I interferons. Cell Cycle. 2006; 5:804–807. [PubMed: 16582590]

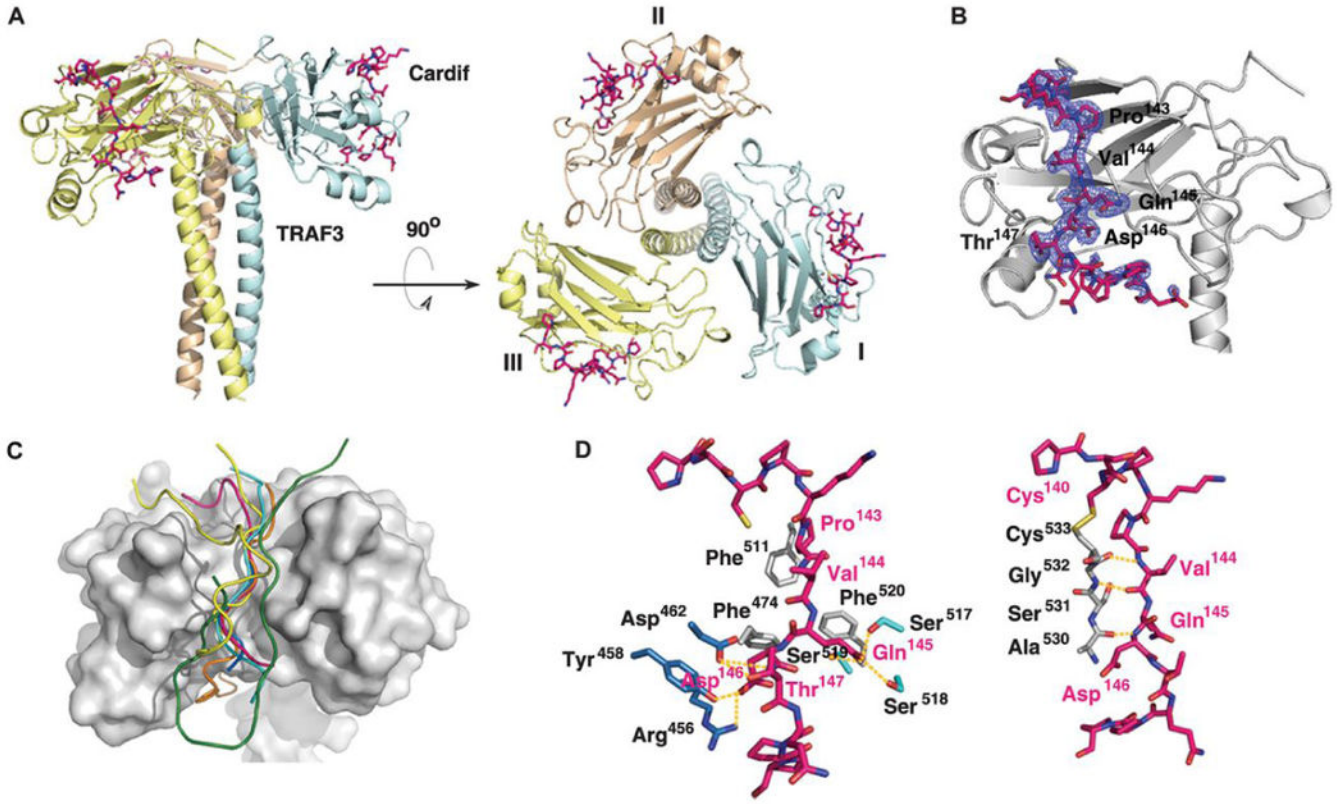

Fig. 1.

Structure of the TRAF3-Cardif complex. (**A**) Representation of TRAF3 homotrimers, shown from both side (left) and top (right) views. The Cardif peptide is in lavender. (**B**) Electron density map of Cardif bound to TRAF3. The blue meshwork represents the $2F_o - F_c$ electron density map contoured at 1.2. TRAF3 is gray; the Cardif peptide backbone is lavender. Cardif residues ^{143}PVQDT^{147} are labeled. (**C**) Different peptides binding to TRAF3. The surface of TRAF3 is gray; peptides shown are from Cardif (lavender), CD40 (green), TANK (cyan), LTβR (yellow), LMP1 (blue), and BAFF-R (orange). (**D**) Molecular TRAF3-Cardif interactions. Key TRAF3-Cardif interactions are shown by yellow dotted lines. Conserved hotspot residues—the hydrophobic patch, serine fingers, and polar residues —are in gray, cyan, and blue, respectively. For clarity, only one of the alternative confirmations of Cardif is shown in (A) and (D).

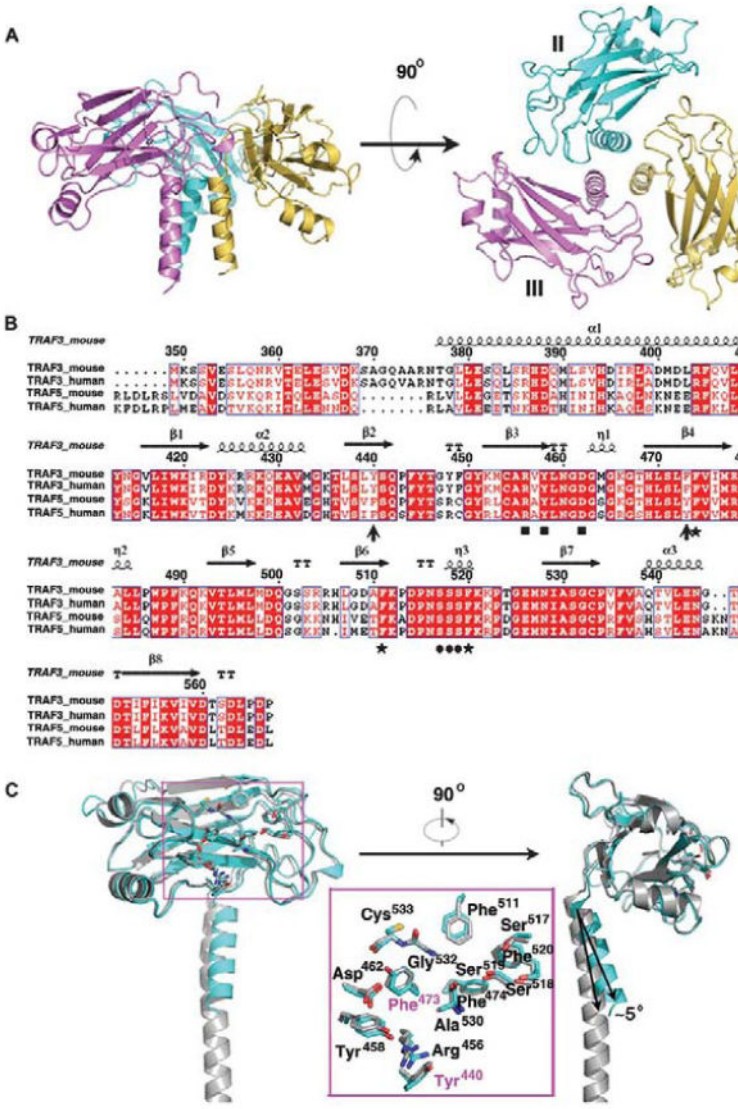

Fig. 2.

Structural comparison of TRAF5 and TRAF3. (**A**) Representation of TRAF5 homotrimers. (**B**) Sequence alignment of the TRAF domains of TRAF3 and TRAF5. The hotspot residues in the hydrophobic patch, serine fingers, and polar residues are labeled as stars, dots, and squares, respectively. The amino acids that play crucial roles in “switching” TRAF5 to TRAF3 are highlighted by black arrows. (**C**) Superposition of TRAF3 and TRAF5 structures. TRAF3 is gray, and TRAF5 is cyan. Conserved hotspot residues, Phe^{473} and Tyr^{440} in TRAF3 and Tyr^{462} and Phe^{429} in TRAF5, are shown within the magnified insert.

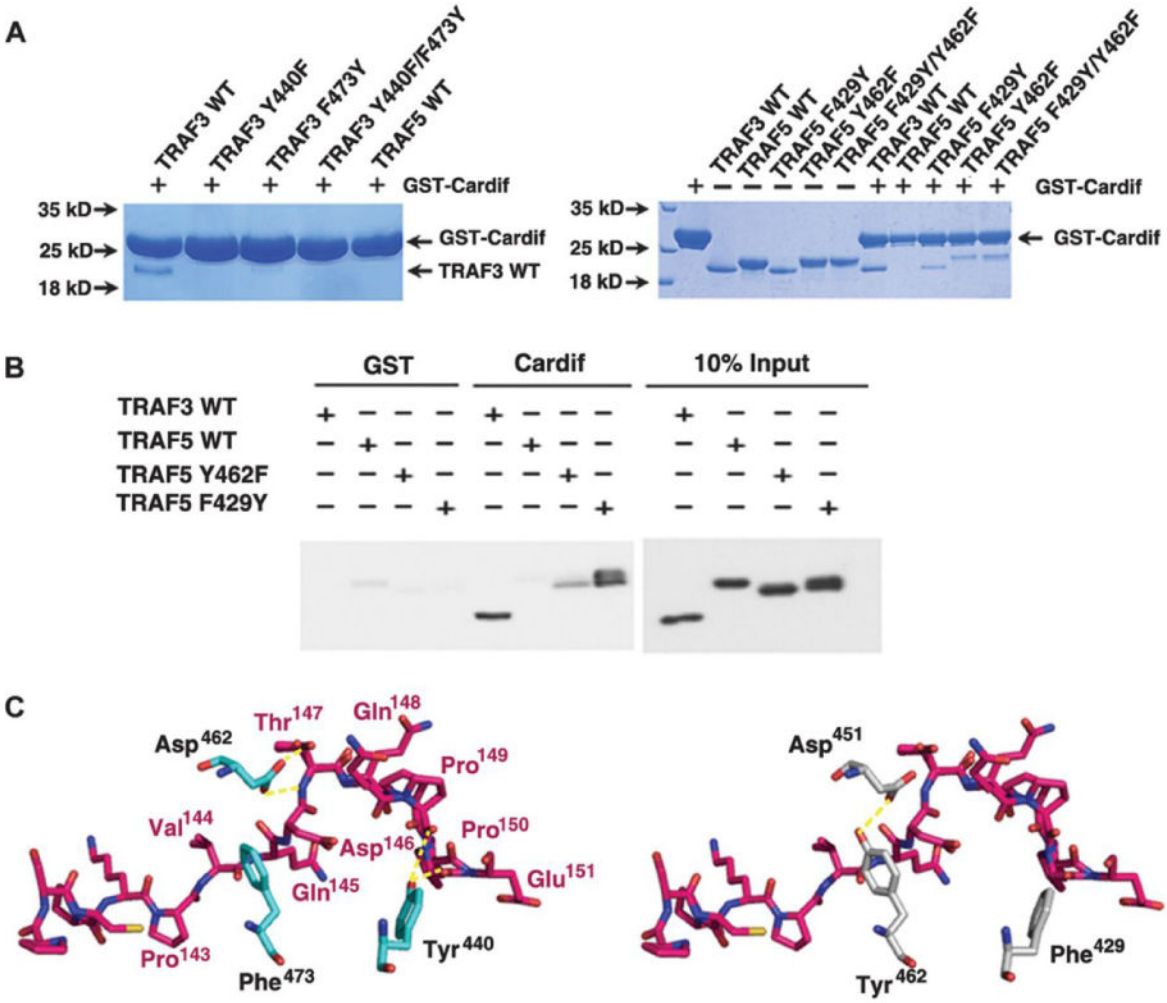

Fig. 3.

Tyr^{440} and Phe^{473} in TRAF3 are necessary for interaction with Cardif. (**A**) Immunoblot analysis of interactions between a 13-residue Cardif peptide (residues 138 to 150) and the TRAF domains of wild-type (WT) TRAF3, WT TRAF5, TRAF3 mutants (left), and TRAF5 mutants (right). (**B**) Lysates from cells expressing FLAG-tagged WT TRAF3, WT TRAF5, TRAF5 Y462F, and TRAF5 F429Y constructs were immunoprecipitated with GST-Cardif TIM and immunoblotted for the FLAG epitope. (**C**) The presumed interactions (orange dotted line) between TRAF3 (left) and Cardif are absent in TRAF5 (right). Results in (A) and (B) are confirmed by three independent experiments.

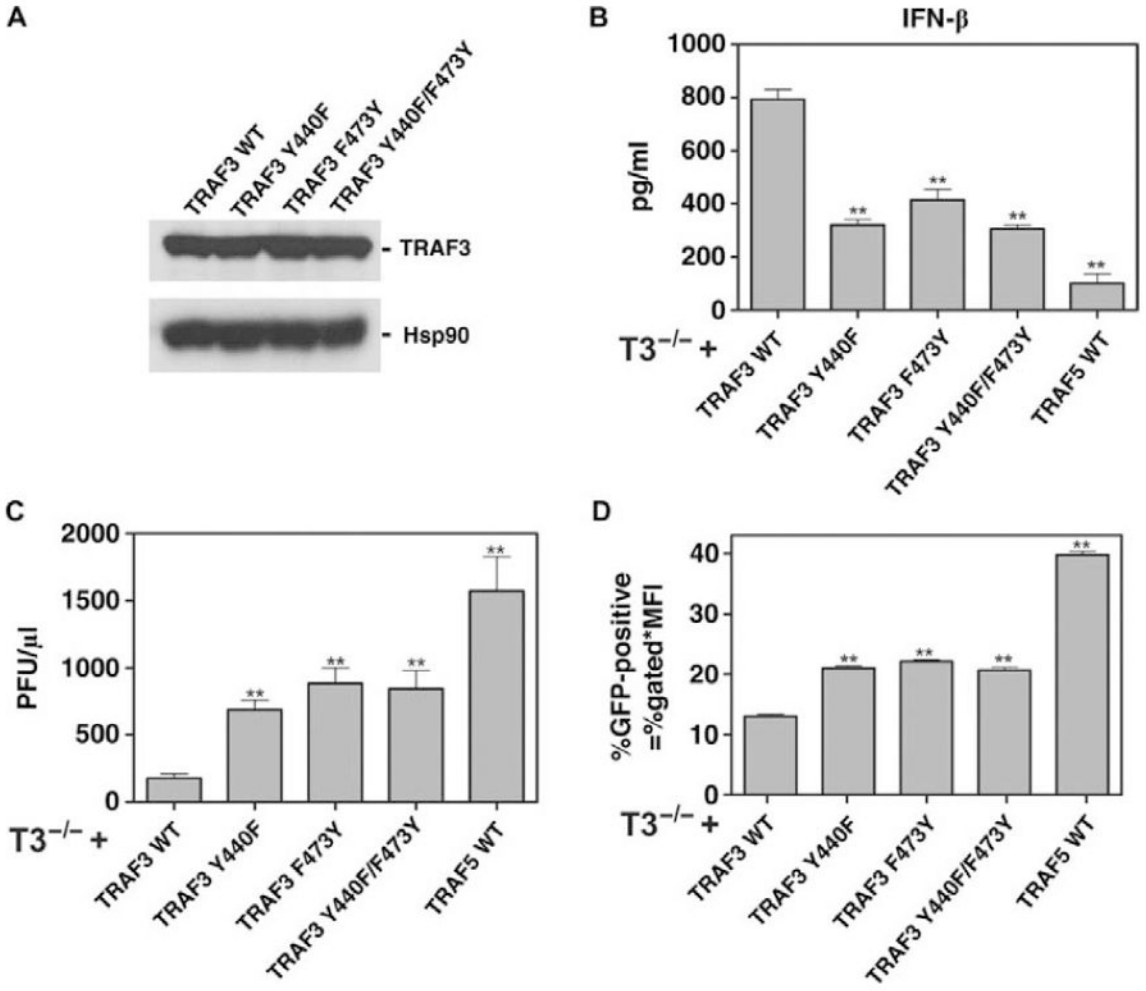

Fig. 4.

TRAF3 Y440F and F473Y lose antiviral function. (**A**) Immunoblot of *TRAF3*−/− MEFs reconstituted with WT TRAF3, WT TRAF5, TRAF3 F440Y, TRAF3 Y473F, or TRAF3 F440Y/Y473F. (**B**) IFN-β production was assessed in reconstituted *TRAF3*−/− MEFs infected with VSV-GFP. (**C**) Viral titer was assessed in reconstituted *TRAF3*−/− MEFs infected with VSV-GFP (**D**). VSV-GFP fluorescence was quantified and calculated by the product of the percent GFP-positive cells and the geometric mean fluorescence intensity of GFP. Results represent an average of three independently analyzed biological replicates and were confirmed by three separate experiments. Error bars indicate the SD. Unpaired *t* test (two-tailed), $n = 3$. *$P < 0.05$; **$P < 0.01$.

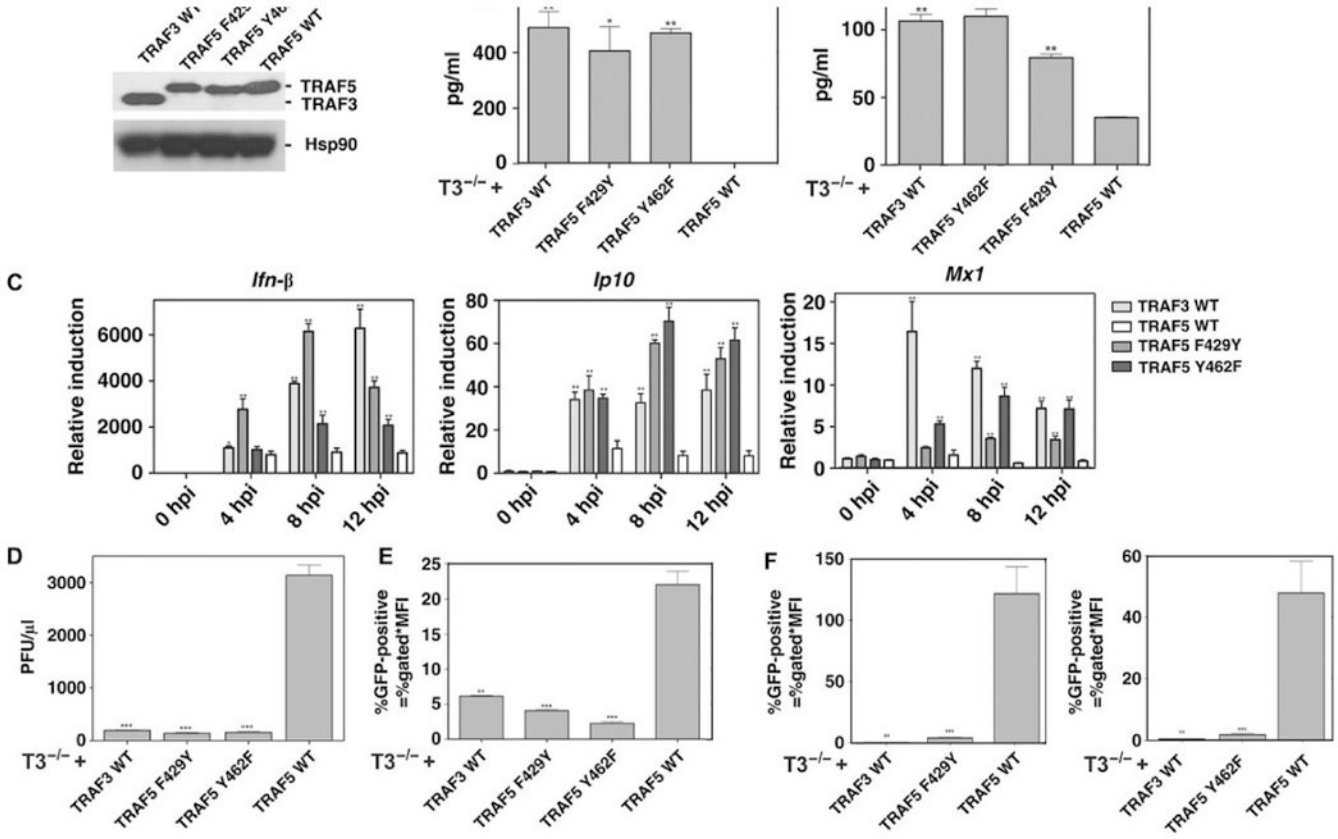

Fig. 5.

The TRAF5 Y462F and F429Y mutants gain TRAF3-like antiviral function. (**A**) Immunoblot of *TRAF3*−/− MEFs that were reconstituted with WT TRAF3, WT TRAF5, TRAF5 F429Y, TRAF5 Y462F, or vector. (**B**) IFN-α production by Sendai virus–infected reconstituted *TRAF3*−/− MEFs and IFN-β production by VSV-GFP–infected reconstituted *TRAF3*−/− MEFs. (**C**) mRNA was collected at 0, 4, 8, and 12 hours after infection with VSV-GFP and assayed by quantitative polymerase chain reaction for induction of *IFN*-β, *IP10*, and *MX1*. (**D** and **E**) Viral titer was assessed in reconstituted *TRAF3*−/− MEFs infected with VSV-GFP (D). VSV-GFP fluorescence was quantified (E). (**F**) Single-cell clones were generated from stably reconstituted *TRAF3*−/− MEFs. GFP fluorescence was determined in cells infected with VSV-GFP. Single-cell clones from cells reconstituted with TRAF5 F429Y (left) and Y462F (right) were tested in separate experiments. Plots represent average GFP fluorescence of three single-cell clones per construct. All results represent an average of three biological replicates and were confirmed by three separate experiments. Error bars indicate the SD. Unpaired *t* test (two-tailed), $n = 3$. **P* < 0.05; ***P* < 0.01.

Table 1

Data collection and refinement statistics (molecular replacement).

TRAF3-Cardif	**TRAF5**	
	Data collection	
Detector	SSRF 17U	KEK BL5A
Space group	$P32_1$	$P2_12_12_1$
Cell dimensions		
a, *b*, *c*(Å)	83.491, 83.491, 78.194	71.053, 90.579, 117.216
α, β, γ(°)	90, 90, 120	90, 90, 90
Resolution (Å)	2.20 (2.20−2.24)*	2.80(2.80−2.85)*
R_{merge}	0.185(0.689)	0.169(0.503)
$\|\|\sigma\|$	16.84(2.74)	18.8(5.5)
Completeness (%)	99.9(100)	93.8(100)
Redundancy	6.9(5.9)	10.5(11.0)
	Refinement	
Resolution (Å)	2.20−36.8	2.80−33.1
No. reflections	15,312	16.783
R_{work}/R_{free}	0.178/0.223	0.224/0.273
No. atoms		
Protein	1,651	4,228
Ligand/ion	0	0
Water	151	44
B-factors		
Protein	33.0	50.7
Water	33 5	32.8
RMSDs		
Bond lengths (Å)	0.007	0.011
Bond angles (°)	1.042	1.156

*Values in parentheses are for the highest-resolution shell.